ELSEVIER

Applied Catalysis A: General 169 (1998) 299–313

APPLIED CATALYSIS A: GENERAL

Evaluation of commercial FCC catalysts for hydrocarbon conversion I. Physicochemical characterization and *n*-hexane conversion

A. Brait, K. Seshan, J.A. Lercher*

Department of Chemical Technology, Catalytic Processes and Materials, University of Twente, PO Box 217, 4500 AE Enschede, The Netherlands

Received 19 July 1997; received in revised form 27 December 1997; accepted 29 December 1997

Abstract

The physicochemical properties of six steam-stabilized, commercial FCC catalysts were compared in respect of their catalytic activity for *n*-hexane conversion. The conversion of *n*-hexane over these catalysts could be fully explained by three reaction pathways: protolytic cracking, protolytic dehydrogenation and hydride transfer. Matrix components did not contribute to the *n*-hexane conversion. A correlation of the acid strength distribution, measured by pyridine TPD showed that nearly all sites with high acid strength are located in the micropores of the zeolite component. ^{27}Al–MAS–NMR distinction between octahedral-, tetrahedral- and pentacoordinated species seems to be unsuitable for the determination of different tetrahedral species in this kind of catalysts. The introduction of rare-earth metals into the zeolites increases the acid strength of the active sites manifested in sequential reactions of the primary formed alkyl surface species, i.e. β-scission and hydride-transfer reactions. The addition of water to the reactant stream decreases the conversion due to competitive adsorption, but does not change the amount, nor the nature of the active site. © 1998 Elsevier Science B.V.

Keywords: Fluid catalytic cracking; Catalysts; Faujasite; Reaction pathways; Water addition

1. Introduction

Fluid catalytic cracking (FCC) is one of the largest-scale processes involving catalysts in a refinery. It is the conversion of long-chain hydrocarbons into smaller molecules, primarily of the gasoline boiling point range. Zeolite based catalysts have been used in the process for over thirty years. These catalysts contain a faujasite-type zeolite as the major active component, embedded in a silica and/or alumina matrix. This matrix acts as a binder, serves as a diluting medium, provides large mesopores for diffusion to the active zeolite crystal and facilitates heat transfer during cracking reactions [1].

Despite the fact that these catalysts have been in use for such a long time, fundamental data of structure–activity relationships are scarce. One reason for this is the large number of elementary reactions that occur (both parallel and consecutive) when cracking complex feedstocks, such as protolytic cracking, dehydrogenation, β-scission, cyclization, oligomerization, coking or hydride transfer [2]. Another reason is the large amount of different molecules present in the vacuum gasoil feed, which can react according to

*Corresponding author. Fax: +31-(0)53-489 4683; e-mail: j.a.lercher@ct.utwente.nl

PII S0926-860X(98)00023-4

these reaction pathways. Hence, significant effort is undertaken to predict FCC catalyst performance by using model components (*n*-hexane, *n*-octane, *n*-hexadecane, cumene, cyclohexane, etc.) as feed [3–5]. This lowers the number of different reactions and allows to describe catalytic activity in terms of different reaction pathways, e.g. cracking via carbonium- or carbenium-ion routes, and relate these activities to physicochemical properties of the catalysts. Conceptually, it should be possible to derive basic structure–activity relationships which should finally lead to rational FCC catalyst design [2].

In this work, *n*-hexane was chosen as a model compound for evaluating FCC catalyst performance. *n*-Hexane is already used for catalyst characterization in industry (in the so-called α-test [6]) and it is a relatively simple molecule, which yields a limited number of reaction products. Moreover, we have had extensive experience of its conversion over well-defined zeolites [7–9]. Thus, we should be able to correlate between physicochemical characteristics of the FCC catalysts and reaction pathways induced. The knowledge of these relationships is expected to improve the selection procedure for FCC catalysts. By comparing with the standard MAT test, links to current selection procedures will be made.

In the present work, we have compared the physicochemical characterization of various commercial steam-stabilized FCC catalysts and *n*-hexane conversion over these catalysts. The results of the catalytic conversion of *n*-hexane will be compared to its conversion over model catalysts. In the second part of this work [10], we compare *n*-hexane conversion to the widely used micro-activity test (MAT) and describes the time-on-stream (TOS) behavior of these FCC catalysts.

2. Experimental

Six steam-stabilized commercial FCC catalysts have been studied. Steam stabilization was carried out at 1023 K for 17 h in a fixed bed using 100% steam.

For the physicochemical characterization, XRD (unit-cell size, relative crystallinity), temperature-programmed desorption (TPD) of pyridine (acidity distribution), XRF (aluminum, silicon and rare-earth content), N_2 ad/desorption (external surface area and micropore volume as well as zeolite content) and ^{27}Al–solid-state–MAS–NMR (distribution of framework and extra-framework alumina) measurements were done.

The *X-ray diffractograms* were measured with a step scan of 0.25°/min for $15<2\theta<35°$, using CuK_α-radiation (0.15418 nm) at 40 kV/30 mA. Silicon powder was added as an internal standard (0.05 g for 1.5 g of catalyst) and the samples were prepared as self-supporting wafers. In the measured region the following reflections were used to estimate the unit-cell size: (331), (333/511), (440), (533) and (642). Additional reflections were used if present: (551/711), (733), (660/822), (555/751), (840), (664) and (931). The unit-cell size was calculated according to the ASTM-method D3942-91.

For *pyridine TPD* the sample was evacuated and held at 861 K for 1 h. Then, it was cooled to 373 K and pyridine was adsorbed for 1 h ($\sim$10 mbar) at this temperature. After evacuation, the sample was heated to 423, 523, 623 or 723 K and held for 1 h. TPD spectra were recorded starting at these evacuation temperatures up to 1013 K at a heating rate of 10 K min^{-1}. Detection of the desorbing species was done by mass spectrometry. This procedure allowed the estimation of the concentration of acid sites with different acid strengths [11].

The *XRF measurements* were carried out using a Philips PW 1480 spectrometer with CrK_α-radiation and 50 mV/50 mA. The measured lines were: AlK_α, SiK_α, TiK_α, FeK_α, LaL_α, CeL_α, PrL_β and NdL_β. For the measurements, the samples were prepared by melting the catalyst sample with tetraboric acid into a pearl.

The *external surface areas and the micropore volumes* of the catalysts were measured with a Micromeritics ASAP 2400 by ad/desorption of N_2 at liquid nitrogen temperature. Prior to the measurements the samples were degassed at 573 K for 12 h. Micropore volumes and external surface areas were calculated from the corresponding *t*-plots [12,13].

^{27}Al solid-state–MAS–NMR-measurements were done on a Varian Unity WB 400 spectrometer (frequency of 104.22 Mhz for ^{27}Al) and a spinning rate of the rotor of 7 kHz. A five-degree pulse was applied and 512 scans were accumulated for one spectrum. Standardization was done with $AlCl_3$.

Catalytic testing was performed in a tubular quartz plug-flow reactor. Experiments were done in the stationary mode (residence time experiments) and non-stationary mode (pressure-transient, TOS experiments). For TOS measurements, the carrier gas was switched from pure He to He containing *n*-hexane, while leaving all other parameters constant. Pressure variations during switching the feed gases were in the 10–20 mbar range.

The reactant mixture contained 5% *n*-hexane in He and was converted at 788 K at a pressure of 1.5–2 bar, and a gas flow of 20–75 ml min^{-1} (at STP). The mass of catalysts used was between 0.25–1 g. The WHSV varied between 0.24–3.7 h^{-1} (g *n*-hexane) (g catalyst)$^{-1}$. Additional experiments were carried out, for which water was co-fed (0.5%) to the reactant via a syringe pump. Thermal cracking was estimated by experiments with calcined quartz of the same particle size as the FCC catalysts. These conversions were subtracted from the conversions over the catalysts.

3. Results

The physicochemical properties of the catalysts investigated are summarized in Table 1. The external surface areas of the catalysts were in the 28–60 $m^2\ g^{-1}$ range, with only one catalyst (UTE) exceeding 37 $m^2\ g^{-1}$. The micropore volumes (for pores smaller than 2 nm) were between 3.1–6.2$\times10^{-2}$ $cm^3\ g^{-1}$. The zeolite content calculated from these micropore volumes according to Johnson [14], was in the 12–23% range.

The concentrations of acid sites from which pyridine desorbed at temperatures >623 K (723 K) ranged between 5.1 (1.0)$\times10^{-6}$ and 14.2 (4.4)$\times10^{-6}$ mol g^{-1}. The distribution of acid sites as determined by the desorption of pyridine at various evacuation temperatures is shown for one of the catalysts (UTS) in Fig. 1 and summarized for all catalysts in Table 2.

The Al_2O_3 content of the FCC catalysts varied in the 30–43 wt% range. ^{27}Al-solid-state–MAS–NMR indicated the presence of tetrahedrally (∼60 ppm), octahedrally (∼60 ppm) and pentacoordinated (∼30 ppm) aluminum species. The pentacoordinated species were in the 0–12% range of the total aluminum concentration measured in the catalysts. The contribution of the tetrahedrally coordinated aluminum was between 15–32% and that of octahedrally coordinated aluminum between 24–46%. Due to low symmetry of some extra-framework aluminum, a broad signal was observed in the NMR spectra ranging from Ca. −150 to 200 ppm [15]. This 'low symmetry aluminum' was present in amounts of 32–46%.

The rare-earth content of the FCC catalysts were in the 0.05–1.6 wt% range, calculated as sum of lanthanum-, cerium-, praseodymium- and neodymium oxides. The pure Y-zeolite phases had therefore

Table 1
Physicochemical characteristics of commercial FCC catalysts

Catalyst	UTE	UTA	UTO	UTC	UTS	UTR
External surface area ($m^2\ g^{-1}$)	60	37	34	35	28	32
Micropore volume ($cm^3\ g^{-1}$)	0.062	0.059	0.046	0.048	0.048	0.031
Zeolite content (%)	23	22	17	18	18	12
SiO_2 content (wt%)	59.5	67.1	60.5	62.7	52.2	51.4
Al_2O_3 content (wt%)	36.3	30.1	34.2	32.9	40.2	43.3
Al (tetrahedral) (%)	32	18	17	15	21	20
Al (pentacoordinated) (%)	0	8	5	0	9	12
Al (octahedral) (%)	33	42	46	40	24	30
Al (low symmetry) (%)	35	32	32	45	46	38
RE_2O_3 content (wt%)	0.43	0.05	0.42	0.38	1.60	0.53
Al/unit cell (molecules)	7.4	5.1	8.5	9.7	9.7	1.7
Pyr/unit cell (>623 K)	0.38	0.27	0.41	0.52	0.91	0.57
Unit-cell size (nm)	2.427	2.425	2.428	2.428	2.429	2.422
N-Hexane conversion at 788 K (mol%)	1.0	0.40	0.60	0.87	1.54	0.68

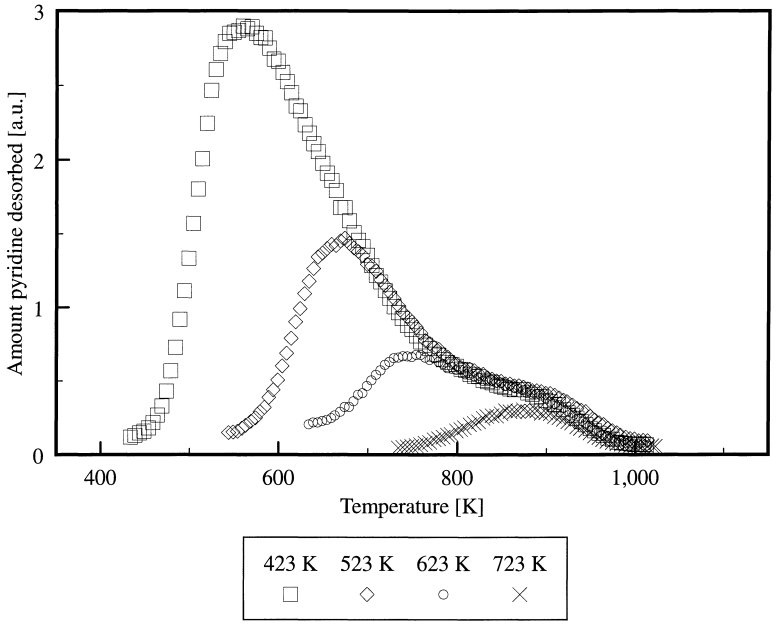

Fig. 1. TPD of pyridine on catalyst UTS recorded for different evacuation temperatures.

Table 2
Concentration of acid sites desorbing pyridine at various temperatures for FCC catalysts

Desorption temperature of pyridine (K)	Catalysts concentration of acid sites $\times 10^6$ (mol g^{-1})					
	UTE	UTA	UTO	UTC	UTS	UTR
423–523	18	8.5	11	13	19	9.5
523–623	11	5.0	8.1	8.9	20	8.8
623–723	4.7	4.1	3.6	5.1	9.8	3.9
723–1013	2.8	1.0	2.5	3.0	4.4	2.0

rare-earth contents ranging from zero (0.23 wt% for UTA) up to 8.9 wt% RE_2O_3 for UTS.

The unit-cell sizes of the catalysts ranged from 2.422 to 2.429 nm and covered a large range of FCC catalysts used for maximizing octane or gasoline in the FCC unit [16]. The catalysts showed, thus, a large difference in their framework aluminum content, which ranged from 2–10 aluminum atoms per unit cell (corresponding to Si/Al ratios of 19–110). This was calculated from the unit-cell size according to Kubelkova et al. [17]. The framework aluminum (FAL), which substitutes for silicon tetrahedral atoms in the lattice, is the cause for Brønsted acid sites in the zeolite structure [2]. Thus, the acid site concentration and the catalytic activity varied almost by a factor of four among the samples investigated.

Rapid initial deactivation of the FCC catalysts with TOS made it difficult to directly compare conversion results. Therefore, conversion was used long after TOS, when the catalyst activity was only slightly changing and it showed a similar linear deactivation for all catalysts. Varying conversion was achieved by changing contact times. A comparison of the different product selectivities at the same *n*-hexane conversion is shown in Table 3. Conversions at short TOS and the variation of *n*-hexane conversion with TOS are presented in Ref. [10].

The energy of activation was estimated for the cracking of *n*-hexane in the 773–873 K range. The conversion of *n*-hexane was adjusted between 2.5–5 mol% by changing the space velocity. The overall energy of activation for the conversion of *n*-hexane was 141 ± 8 kJ mol^{-1}, with an energy of activation for protolytic cracking of 134 ± 5 kJ mol^{-1} and that of dehydrogenation 152 ± 14 kJ mol^{-1}. The hydride-transfer reaction showed an energy of activation of 149 ± 14 kJ mol^{-1}.

Table 3
Product selectivities for *n*-hexane conversion over different FCC catalysts at 788 K and *n*-hexane conversion of 0.6–0.7 mol% at long TOS (5400 s)

Catalyst	UTE	UTA	UTO	UTC	UTS	UTR
Product selectivities (*mol%*)						
Methane	3.1	2.1	3.5	2.7	3.5	4.2
Ethane	6.3	6.6	6.7	6.6	6.3	7.7
Ethene	6.7	6.4	8.2	5.9	6.2	7.8
Propane	7.5	8.2	7.0	7.9	7.5	7.7
Propene	42.5	35.8	43.4	41.7	44.0	44.3
Isobutane	1.6	1.1	0.8	2.0	1.7	1.3
N-Butane	3.8	4.3	3.2	4.1	3.6	3.3
Butenes	9.9	11.5	10.7	10.2	9.3	9.8
Butadiene	<0.1	0.1	0.2	<0.1	<0.1	<0.1
Isopentane	1.6	1.1	0.7	2.1	2.0	1.6
N-Pentane	0.1	0.1	0.1	0.1	0.1	0.1
Pentenes	2.3	2.5	2.6	2.9	2.0	1.9
Isohexanes	5.2	4.4	2.3	5.0	5.3	4.9
Hexenes	9.6	15.8	10.6	8.9	8.5	5.3
Rate of reaction$\times 10^9$ (*mol* g^{-1} s^{-1})						
Dehydrogenation	9.7	5.3	6.9	9.0	16.2	6.0
Protolytic cracking	6.6	3.2	4.3	6.5	11.7	5.6
Hydride transfer	2.7	1.0	0.8	2.8	5.1	1.9

The most abundant product in the reaction of *n*-hexane is propene (36–44 mol%). The other alkenes were formed with selectivities in the 17–30 mol% range. Isoalkanes showed selectivities between 1–2 mol% for isobutane and isopentane and 2–5 mol% for isohexanes. The *n*-alkanes had selectivities from 2–4 mol% for methane and *n*-butane, and from 6–8 mol% for ethane and propane. In contrast, *n*-pentane was never observed in selectivities >0.1 mol%.

The products are ascribed to the different reaction pathways, i.e., protolytic cracking, dehydrogenation and hydride transfer as suggested by Narbeshuber [9]. The rate for protolytic cracking (α-scission, carbonium-ion cracking) was calculated by summation of the rates of *n*-alkane formation from C_1–C_4, while hydride transfer was calculated by summation of all the isoalkanes formed plus *n*-pentane. *n*-Pentane cannot be formed by α-scission, because its formation would require a methyl carbenium ion remaining on the surface. For dehydrogenation, the sums of the reaction products of the primary formed hexenes, i.e. propene and butene/ethene, were added to the rate of hexenes formation. For this purpose, the difference between propane and propene (which should be zero if only protolytic cracking occurred) was taken, and the part, which originated from further cracking of pentenes, was subtracted. For scission of hexenes into butene/ethene, the difference between butenes and ethane was used.

For protolytic cracking and dehydrogenation rates between $3.2–12\times10^{-9}$ mol g^{-1} s^{-1} and $5.3–16\times10^{-9}$ mol g^{-1} s^{-1} were observed, respectively. The lowest rates were observed for the hydride-transfer reaction varying from $0.8–5.1\times10^{-9}$ mol g^{-1} s^{-1}.

In additional experiments, the influence of water on the hydrocarbon conversion was investigated. Generally, we found a lower reaction rate in the presence of water for all catalysts investigated, with the exception of UTS. This catalyst did not change its activity for the protolytic cracking, when water was co-fed.

Pretreatment of the FCC catalysts with water prior to the *n*-hexane conversion did not induce differences in activity compared to the untreated catalyst. Switching between a *n*-hexane/water mixture and *n*-hexane alone in one experiment at different TOS showed no different results compared to the two single runs, indicating complete reversibility of the effect of water. The decreases in the rates were up to 60% of the rates, when no water was co-fed.

4. Discussion

4.1. Physicochemical characterization

Pentacoordinated aluminum was reported [18] to appear with steaming of the zeolite. The fact that this species was not found in the steamed samples, UTE and UTC, suggests that factors other than steam treatment seem to play a role in the formation of pentacoordinated extra-framework aluminum (EFAL) species. Correlations to catalytic properties of the catalysts were not found, showing that this aluminum species is insignificant for the catalytic performance of the FCC catalysts.

The aluminum species with a low symmetry that produce a broad signal in the NMR spectrum are present in very high concentrations due to the high degree of steam dealumination these catalysts have undergone. This feature was also observed by Kellberg et al. [19] and they found it especially pronounced in strongly dealuminated samples. According to these authors, the 'low symmetry' aluminum species are part of all extra-framework resonances and their quadrupolar interactions. They recommended ultrahigh spinning speeds in NMR measurements to get quantitative information about the extra-framework aluminum. At these conditions, the broad signal decreases and the intensities of the other peaks increase by different percentages. Their measurement conditions, however, could not be realized by our measurement conditions.

The octahedral coordinated aluminum in the catalysts stems to a large extent from the silica/alumina matrix in the FCC catalysts. Additionally, some of these octahedrally coordinated aluminum species are formed during the steam dealumination process within the micropores of the zeolites by extracting tetrahedral coordinated framework aluminum out of the lattice.

The tetrahedrally coordinated aluminum comes from two contributions, i.e. from aluminum atoms replacing silicon in the zeolite lattice and from extra-lattice silica/alumina species in the micropores of the zeolite and the matrix. By estimating the content of FAL in an ideal faujasite unit-cell structure H_xAl_x-$Si_{192-x}O_{384}$ (x=2–10) and taking into account the percentage of zeolite in the FCC catalysts, we can calculate the percentage of FAL in comparison to the aluminum content of the FCC catalysts. For the catalysts investigated, we found a contribution of FAL to the total aluminum concentration between 0.20–2.1% only, compared to 15–32% measured by NMR for the tetrahedrally coordinated aluminum. Therefore, most of the tetrahedrally coordinated aluminum found with NMR is due to EFAL species in the zeolite micropores or in the matrix. A separation of the tetrahedral peak at 60 ppm into the contributions of FAL and EFAL was impossible, probably due to their close positions to one another.

In view of the complex structure of the FCC catalysts, especially after severe steaming treatment and the large contributions of the FCC catalyst matrix ^{27}Al–MAS–NMR does not seem to be an appropriate tool to obtain information about the different tetrahedrally coordinated aluminum species in various FCC catalysts. Adsorption of probe molecules or the use of cross-polarization experiments may be a possible way to obtain the necessary information about framework and extra-framework species.

In order to compare the different matrices in the FCC catalysts, the SiO_2/Al_2O_3 ratio of the matrix was determined by assuming an initial Si/Al ratio of 2.5–5 for the zeolite component. The concentration of SiO_2 in the matrices was then found to be between 53–68 wt% by assuming a zeolite with an initial Si/Al ratio of 2.5 and between 50–64 wt% for one with an initial Si/Al ratio of five. This shows that the calculation is not very sensitive to the Si/Al ratio of the catalyst and can be taken as a good estimate of the silica/alumina ratio in the matrix. The Si/Al ratio in all catalyst matrices investigated did not show very large deviations. Thus, we tentatively conclude that in these FCC catalysts a possible catalytic activity of the matrix depends on the specific surface area of the matrix and the amount of pores and not on the concentration of aluminum in the matrix.

A comparison of the concentration of acid sites, measured by pyridine desorption at temperatures >623 K per gram catalyst to the concentration of acid sites per micropore volume is shown in Fig. 2. All catalysts with the exception of UTR lie on one line that intercepts the x-axis at the origin. This shows that nearly all sites adsorbing pyridine strongly, i.e. retain pyridine up to temperatures >623 K, are located within the micropores of the zeolite. The deviation of UTR may be due to the rather severe modification of this catalyst by steam dealumination, evidenced by

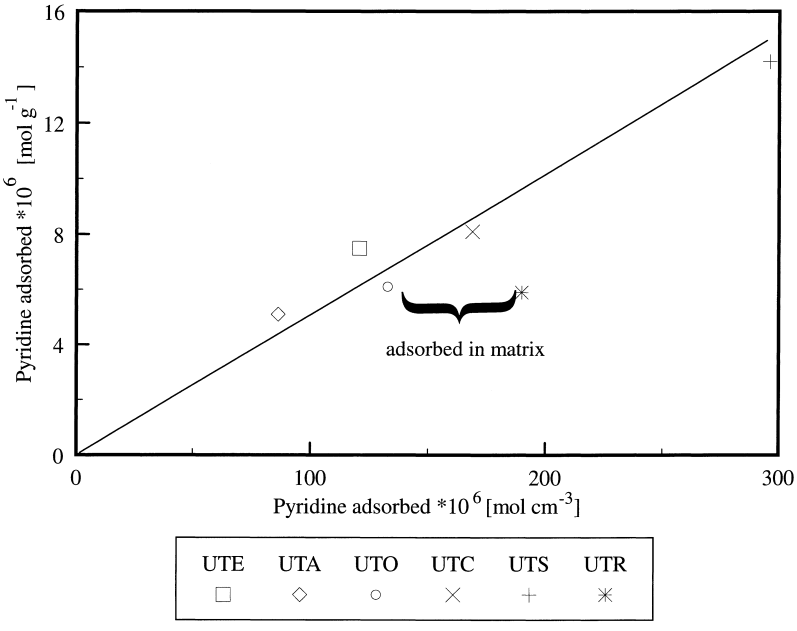

Fig. 2. Pyridine desorbed at temperatures >623 K. Comparison of concentration normalized to gram zeolite and the same normalized to micropore volume.

its low unit-cell size. This seems to lead to more strongly adsorbed pyridine in the mesopores compared to the other catalysts. Subsequently, a normalization of the sites adsorbing pyridine strongly to the micropore volume will lead to an extremely high concentration of acid sites per micropore volume (Fig. 2) compared to all other catalysts.

4.2. Catalytic conversion of n-hexane

In Figs. 3 and 4 the rates of protolytic cracking and dehydrogenation of *n*-hexane conversion at initial TOS, i.e. after 13 s TOS, are compared to the concentration of acid sites which desorb pyridine at temperatures >623 K and 723 K, respectively. At these short TOS, the influence of deactivation was supposed to be negligible. The sites, which retained pyridine at temperatures >723 K showed a better correlation to the protolytic cracking activity. For dehydrogenation, both showed comparable correlations with the exception of the catalyst UTO. A positive intercept of the regression lines with the *x*-axis in these graphs indicates acid sites that are measured by pyridine TPD, but are not active in the respective reactions. For the dehydrogenation (Fig. 4) activity, both regression lines intercept at positive values; therefore, even at a desorption temperature for pyridine of 723 K acid sites are measured, which are not active in dehydrogenation. For protolytic cracking (Fig. 3), the regression line for the acid sites desorbing at temperatures >723 K intercepts at a negative *x*-axis value. In this case, the desorption temperature of pyridine is too high to trace all acid sites active in this reaction. Thus, it is concluded, that for protolytic cracking the sites retaining pyridine after desorption between 623 and 723 K reflect the concentration of active sites, while dehydrogenation is catalyzed by sites that retain pyridine at temperatures >723 K. As strong Lewis acid sites are binding pyridine stronger than Brønsted acid sites [20], it is speculated that Lewis acid sites, probably connected to extra-framework aluminum species, are affiliated with active sites for dehydrogenation.

The dependence of the concentration of pyridine adsorbed at temperatures >623 K on the unit-cell size is shown in Fig. 5. Note that a correlation between the unit-cell size (a measurement of the concentration of aluminum in the zeolite lattice) and the concentration

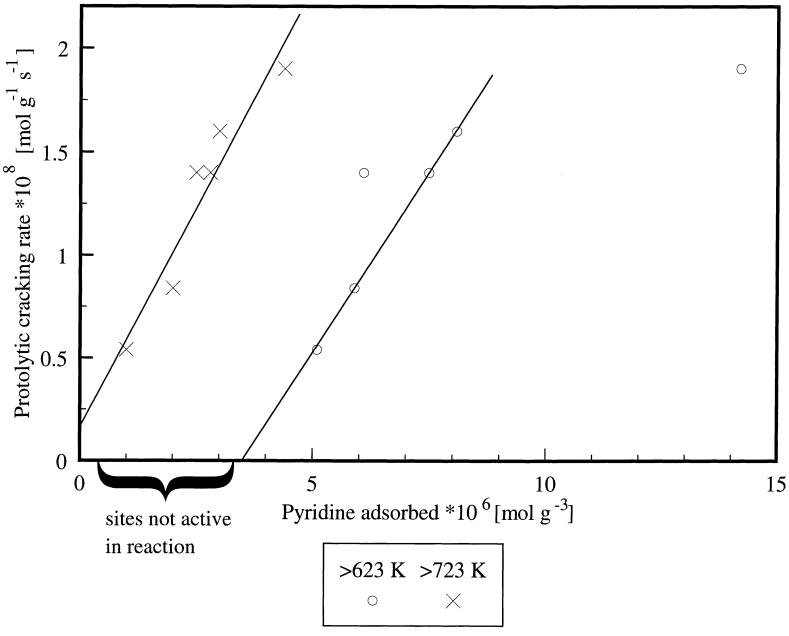

Fig. 3. Protolytic cracking rate vs. concentration of pyridine desorbed at temperatures >623 K and 723 K. Reaction at 788 K, reaction rate at initial TOS, 650 mg catalyst, 50 mbar *n*-hexane.

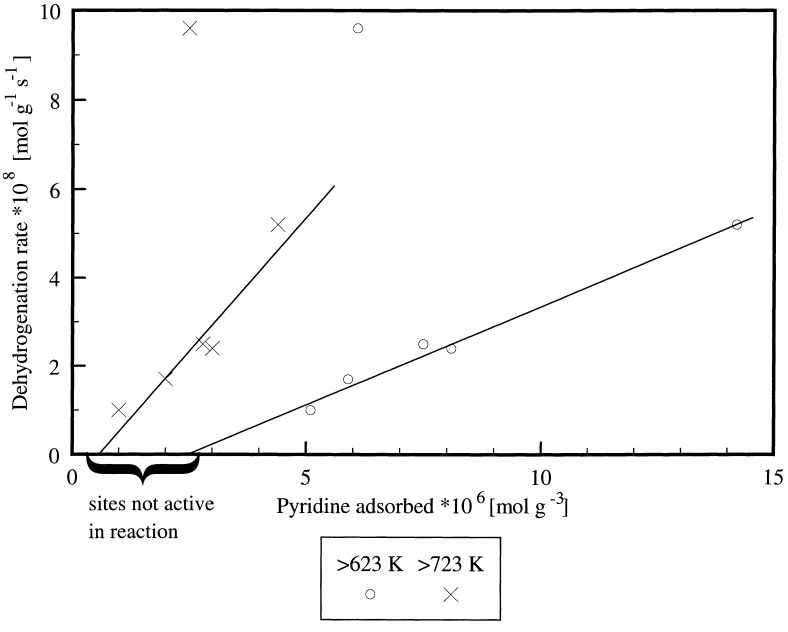

Fig. 4. Dehydrogenation rate vs. concentration of pyridine desorbed at temperatures >623 K and 723 K. Reaction at 788 K, reaction rate at initial TOS, 650 mg catalyst, 50 mbar *n*-hexane.

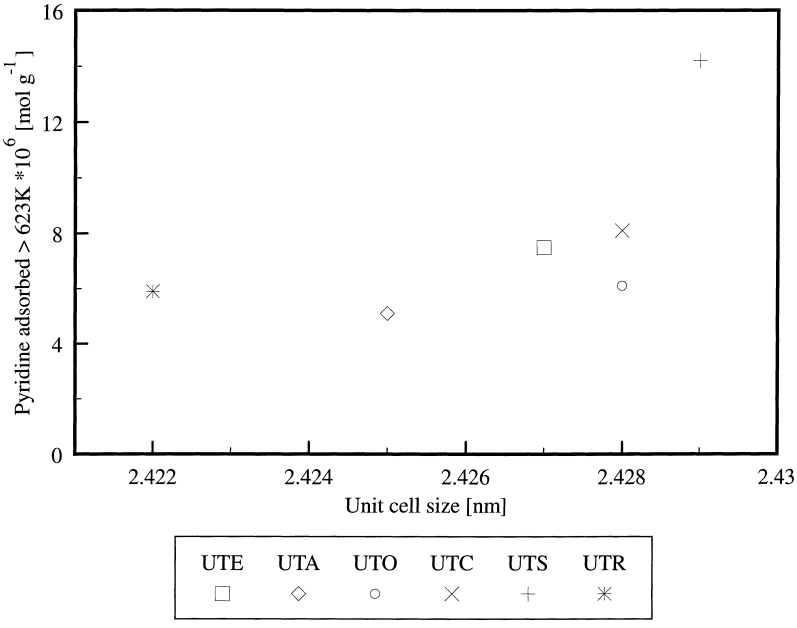

Fig. 5. Correlation of pyridine retained at temperatures higher than 623 K to unit cell size of zeolite component in FCC catalyst.

of active sites responsible for the activity in *n*-hexane conversion was not observed. For further analysis, the concentration of pyridine per unit cell desorbing higher than 623 K was calculated. The values varied between 0.27 and 0.91 pyridine molecules per unit cell (Table 1). A high degree of dealumination in the zeolite produces more EFAL which may block the access to active sites or neutralize them. A comparison with the amount of aluminum per unit cell (Table 1) clearly shows that a large fraction of the tetrahedrally coordinated aluminum sites is covered by EFAL species. One might thus not expect that the concentration of acid sites and, hence, activity in n-hexane cracking correlates with the unit-cell size, which is a measurement of the concentration of tetrahedrally coordinated aluminum atoms in the lattice.

The product distribution in our experiments as shown in Table 3 could be very well explained by carbenium-ion chemistry [2] and protolytic cracking or protolytic dehydrogenation following suggestions by Haag and Dessau [21] and Corma et al. [22]. We considered three different reaction pathways, i.e. protolytic cracking (C–C bond breaking of a carbonium ion), dehydrogenation (C–H bond breaking of a carbonium ion), in which further cracking via β-scission of formed carbenium ions is included, and hydride-transfer reactions [9]. A reaction scheme for these reactions is shown in Fig. 6. By normalizing the sum of these three routes to unity, we obtained reaction path probabilities. The carbonium ion route had a probability of 0.34–0.41 over the various catalysts with reference to C–C bond breaking and, hence, building up of methane/pentenes, ethane/butenes, propane/propene and *n*-butane/ethene. For the C–H bond breaking (dehydrogenation), we found a probability of 0.44–0.58. This route consists of formation of hexenes plus the contribution of hexene cracking via β-scission to yield butenes/ethene or propene. As it is clearly seen from Table 3, most of the intermediately formed hexyl carbenium-ion species are cracked further to yield propene. We could also observe a further cracking of initially formed pentenes to ethene and propene. Hydride transfer (manifested by formation of isobutane, *n*-pentane, isopentane and isohexanes) showed a probability of 0.06–0.16. This low probability is attributed to the low acid site density in the FCC catalysts, the high reaction temperature and low conversions, which do not favor secondary bimolecular reactions. The routes for dehydrogenation and hydride transfer were inversely related. The higher the prob-

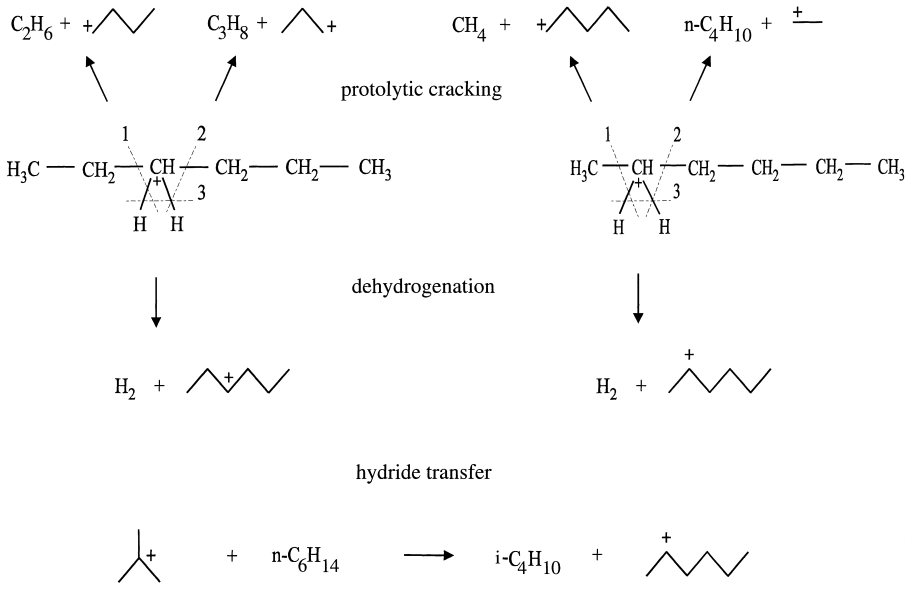

Fig. 6. Reaction pathways for catalytic conversion of *n*-hexane.

ability to dehydrogenation on a particular catalyst, the lower was the probability to hydride transfer, which is shown in Fig. 7. Catalyst UTR deviates from this behavior due to a higher probability for cracking (0.41) in comparison to the other catalysts (0.34–0.36).

The activation energies measured for the overall reaction of *n*-hexane were in agreement with results of Fritz and Lunsford [23] on *n*-hexane conversion over pure HY zeolites, who found values between 142–150 kJ mol^{-1}. Moreover, the activation energies of protolytic cracking and dehydrogenation were in line with the values reported by Narbeshuber et al. [8] over HY zeolites. These results lead to the conclusion that the matrix of the FCC catalysts investigated does not play a significant role in cracking of *n*-hexane and the catalytic activity observed is due to the zeolite component.

A comparison of the different contributions to protolytic C–C cleavage is shown in Fig. 8[1]. Through protolytic cracking, ethane and propane are formed as primary products by cracking the carbonium ion at position C_3, methane and *n*-butane by cracking at position C_2. The higher amount of ethane/propane formed compared to methane/*n*-butane, i.e. 67% compared to 33% shows a preferential formation of the inner carbonium ion, i.e. the carbonium ion on C_3. This may be due to a higher stabilization by two secondary carbon atoms compared to the stabilization due to one primary and a secondary carbon. From the higher selectivity of *n*-butane compared to methane and of propane compared to ethane, a preferential cleavage of the C–C bond – adjacent to central carbon atoms for a particular carbonium ion – was observed for the catalyst without rare-earth-containing zeolite component. For the catalysts containing rare-earth oxides there is no preference to cleave the inner C–C bond and, therefore, to producing more propane than ethane and more *n*-butane than methane.

In Fig. 9, the different contributions to the dehydrogenation pathway are compared. As in protolytic cracking, we note a difference between catalyst UTA, containing a non-rare-earth exchanged zeolite component and the others, which contain rare-earth cations in varying concentrations. In the latter case, the probability to crack hexenes further is ~25% higher. This is in line with the higher acid strength of rare-earth-

[1]Note that in Figs. 8–10 lines are not extended to the non-rare-earth-containing zeolite UTA due to the lack of information on the course of these lines with lower rare-earth content.

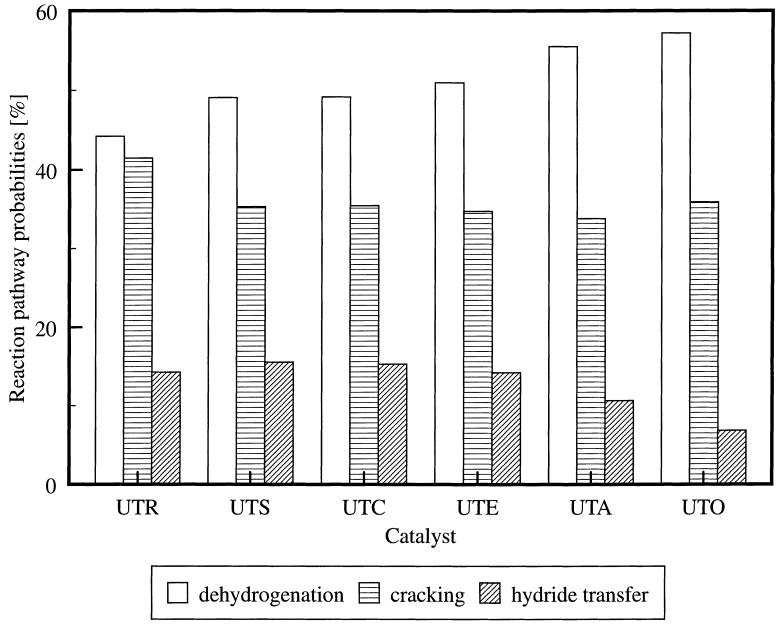

Fig. 7. Reaction pathway probabilities for protolytic cracking, dehydrogenation and hydride transfer over FCC catalysts at 788 K, 50 mbar *n*-hexane and *n*-hexane conversion of 0.65 mol%.

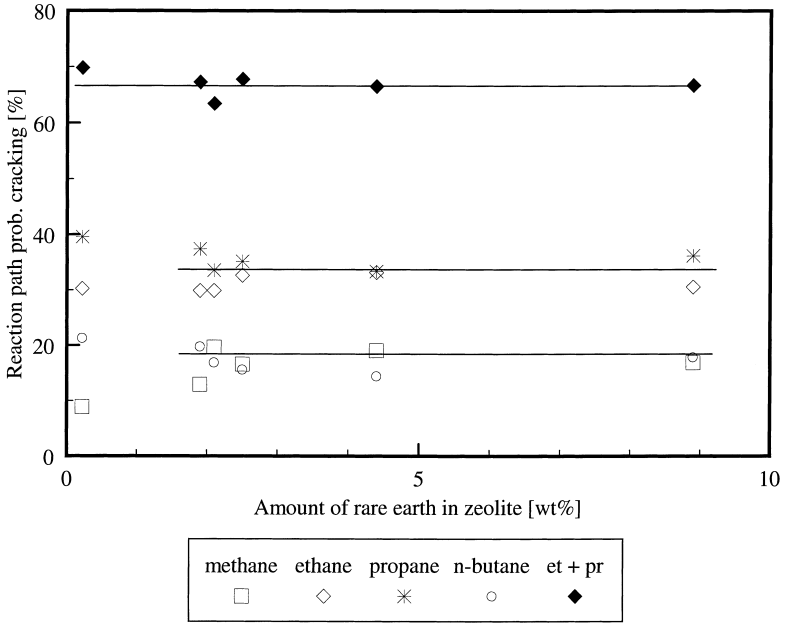

Fig. 8. Reaction probabilites to different products in protylytic cracking over FCC catalysts at 788 K, 50 mbar *n*-hexane and *n*-hexane conversion of 0.65 mol%.

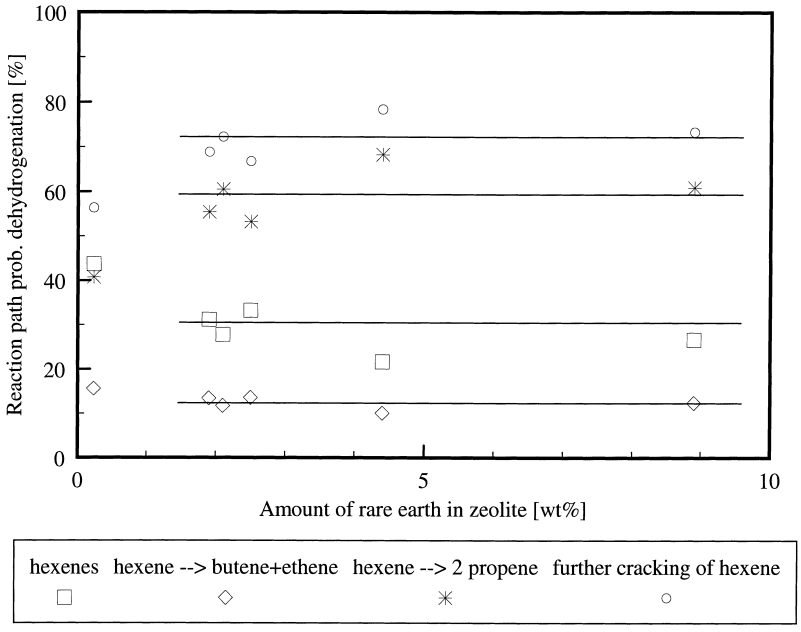

Fig. 9. Reaction probabilities to different products in dehydrogenation over FCC catalysts at 788 K, 50 mbar *n*-hexane and *n*-hexane conversion of 0.65 mol%.

containing zeolites as described by Carvajal et al. [24] due to an electron withdrawal effect of these polyvalent cations from the framework hydroxyl groups, thus, creating more acidic protons. Stronger acid sites will show a stronger interaction with the adsorbed carbenium ion, i.e. a more stable alkoxy group which will lead to a longer residence time of these species on the catalyst surface. This will increase the probability of the secondary β-scission reaction of the hexyl surface species, leading to formation of propene or ethene/butenes. This effect could also be due to a higher adsorption capacity of *n*-hexane in the micropores of the rare-earth-containing zeolites and not to a higher acid strength of the active sites. Adsorption measurements of *n*-hexane on both types of catalysts (UTA, UTC, UTS) did not show significant differences in the adsorption capacity which suggests that it is in fact acid strength and not a difference in the adsorption properties that causes the higher amount of secondary reactions. Cracking via β-scission to form propene has a much higher probability than forming ethene/butenes, which is explained by a preferential cleavage of the carbenium ion at C_2, which leaves a propyl carbenium ion on the catalyst surface. The cleavage of the carbenium ion at position C_3 would result in a remaining ethyl carbenium ion on the surface. This can only be a primary carbocation, which makes this pathway less probable.

In the hydride-transfer reaction (Fig. 10), the very low probability to *n*-pentane is, firstly, a result of the fast rearrangement of the linear *n*-pentyl carbenium ion to branched carbenium ions as compared with the hydride-transfer reaction and, secondly, due to the shorter lifetime of a secondary carbenium ion compared to a tertiary one. Therefore, the isopentyl carbenium ion, which is tertiary, will dominate over the linear pentyl carbenium ion on the catalyst surface and undergo more hydride-transfer reactions, which leads to a higher amount of isopentane. Isohexanes are formed with the highest probability between 52–67%, which is in line with the high dehydrogenation activity and, therefore, high amount of hexyl carbenium ions on the catalyst surface. The same amounts of formed isobutane and isopentane supports the conclusion, that the amounts of isobutyl- and isopentyl carbenium ions on the surface and the hydride-transfer rate to these species are comparable. The slightly higher probability to form isohexanes over catalyst

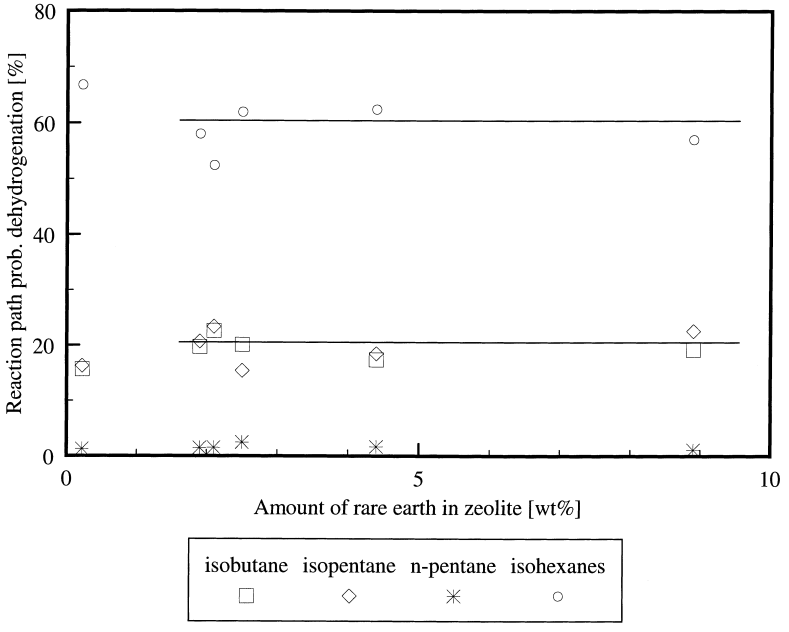

Fig. 10. Reaction probabilities to different products in hydrode transfer over FCC catalysts at 788 K, 50 mbar *n*-hexane conversion of 0.65 mol%.

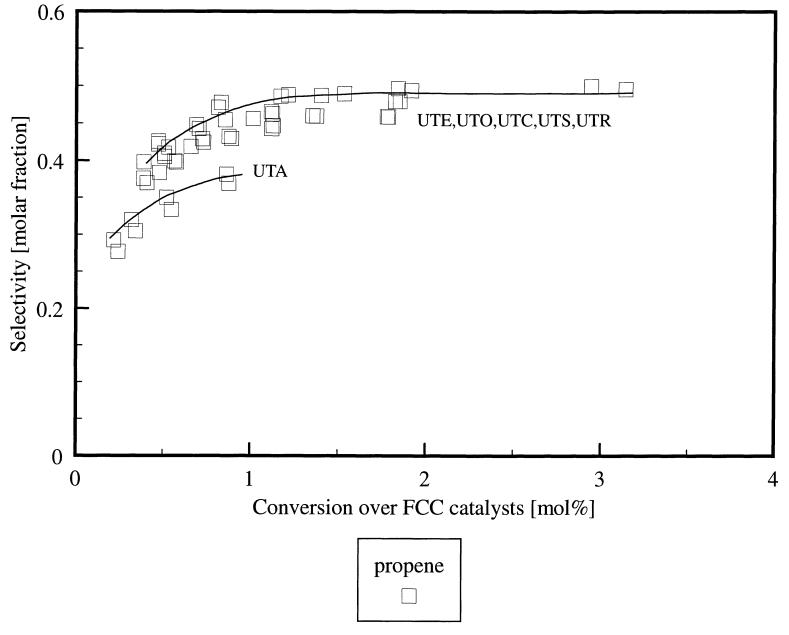

Fig. 11. Selectivity to propene in the conversion of *n*-hexane over FCC catalysts at different conversion levels. Reaction temperature 788 K, 50 mbar *n*-hexane.

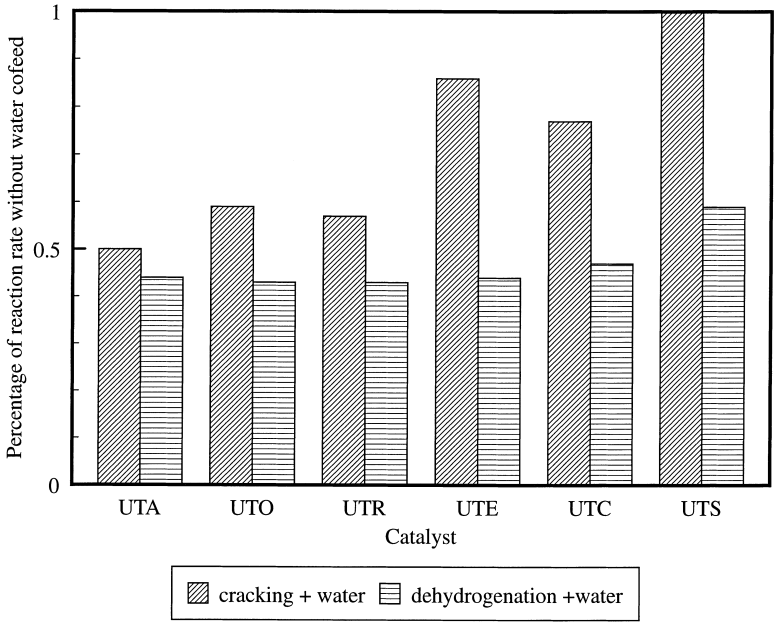

Fig. 12. Influence of co-feeding water on protolytic cracking and dehydrogenation normalized to the rates of reaction without water co-feed. Reaction temperature 788 K, 50 mbar *n*-hexane, 4 mbar water.

UTA (no rare-earth cations) is parallel to the higher amount of hexenes formed in the gas phase over UTA compared to all other catalysts (Table 3).

Comparing the product selectivities in the conversion of *n*-hexane as shown in Table 3, one notes the high selectivity of propene. The higher the conversion, the more propene is formed. This is due to a higher importance of secondary β-scission reactions. However, this reaches a limit at a selectivity to propene of ca. 50%, which is shown in Fig. 11. UTA (no rare-earth cations) deviates from the other catalysts and shows a lower propene selectivity. In that context, it should be suggested that RE-USY zeolites have stronger acid sites than USY zeolites and, therefore, produce more propene, which is formed by further cracking of initially produced hexyl- and pentyl carbenium ions.

Co-feeding water clearly shows that the lower activity of the catalysts in the presence of water is due to competitive adsorption of water on the active sites. It does not, however, change the strength of the acid sites, e.g. by dealuminating the zeolite lattice. In Fig. 12 the rates of protolytic cracking and dehydrogenation are shown, normalized to the rates of reaction, when no water was co-fed. The dehydrogenation pathway was ca. 45% of the activity in the experiment without water, while the decrease in the protolytic cracking pathway strongly differed between the catalysts (50–100%). It is suggested that the sites involved in dehydrogenation are rather uniform in their acid strength and, therefore, show a similar competitive adsorption of water. On the contrary, the sites responsible for protolytic cracking do not seem to be very uniform. Subsequently, the competitive adsorption of water will differ according to the acid strength of these sites. Obviously, protolytic cracking proceeds on sites with a broader range of acid strength than protolytic dehydrogenation, in line with the results of pyridine TPD.

5. Conclusions

The FCC catalysts investigated showed a large difference in unit-cell size, framework-aluminum content and Brønsted acidity. A dependence of the unit-cell size and the concentration of acid sites that retain pyridine at temperatures >623 and 723 K was not found. This is attributed to the high dealumination and different history of the catalysts. A good correla-

tion between the initial catalytic activity and the concentration of acid sites of higher acid strength was observed. The larger part of the catalyst acidity is attributed to weak acid sites that desorb pyridine at temperatures <623 K and which are not significantly active in cracking. The strong acid sites, which are active for catalytic cracking, are mainly located within the micropore structure of the zeolite. From this and the low external surface areas of the catalysts it can be concluded that the matrix plays a minor role in the conversion of *n*-hexane under the reaction conditions employed. This is strongly supported by the measurements of energies of activation which are in line with the values of *n*-hexane conversion over pure HY and RE-HY zeolites.

As with pure Y zeolites, the product distribution can be explained by three different reaction pathways: Protolytic cracking, dehydrogenation as primary reactions and hydride transfer as a secondary reaction. Alkyl surface species show a higher retention on the catalysts containing rare-earth oxides which is attributed to higher stability of the alkoxy group on the surface and higher acid strength. This increases the probability of further cracking of these species (β-scission). Addition of water had a negative influence on the reaction rates due to competitive adsorption of water on the catalytically active sites.

Acknowledgements

We would like to thank the OMV, Austria, for the financial support and interest in this study. Partial support by the Christian Doppler Society is gratefully acknowledged. The help of L. Vrielink with the XRF analyses and V. Skolnik with the N_2 ad/desorption measurements is gratefully acknowledged.

References

[1] J. Scherzer, Octane-Enhancing Zeolitic FCC Catalysts: Scientific and Technical Aspects, Marcel Dekker, New York, Basel, 1990.
[2] A. Corma, B.W. Wojciechowski, Catalytic Cracking, Catalysts, Chemistry, and Kinetics, Marcel Dekker, New York, Basel, 1986.
[3] F.N. Guerzoni, J. Abbot, Catal. Lett. 16 (1992) 53–58.
[4] M. Bassir, B.W. Wojciechowski, J. Catal. 150 (1994) 1–8.
[5] A. Corma, P.J. Miguel, A. Orchilles, Appl. Catal. A: General 117 (1994) 29–40.
[6] J.N. Miale, N.Y. Chen, P.B. Weisz, J. Catal. 6 (1966) 278–287.
[7] T.F. Narbeshuber, H. Vinek, J.A. Lercher, J. Catal. 157 (1995) 388–395.
[8] T.F. Narbeshuber, A. Brait, K. Seshan, J.A. Lercher, J. Catal. 172 (1997) 127.
[9] T.F. Narbeshuber, Thesis, University of Twente, Enschede, 1994.
[10] A. Brait, K. Seshan, H. Weinstabl, A. Ecker, J.A. Lercher, Appl. Catal. A: General 169 (1998) 313–327.
[11] A. Corma, V. Fornés, F.V. Melo, J. Herrero, Zeolites 7 (1987) 559–563.
[12] J.H. De Boer, B.C. Lippens, B.G. Linsen, J.C.P. Broekhoff, A. van den Heuvel, Th.J. Osinga, J. Coll. Interface Sci. 21 (1966) 405–414.
[13] K.S.W. Sing, Chem. Ind. (1967) 829.
[14] M.F.L. Johnson, J. Catal. 52 (1978) 425–431.
[15] H. Pfeifer, in P. Diehl, E. Fluck, H. Günther, R. Kosfeld, J. Seelig (Eds.), NMR-Basic Principles and Progress 31, Solid State NMR II Inorganic Matter, Springer Verlag–Berlin–Heidelberg, 1994, p. 31.
[16] A. Haas, K.E. Finger, U. Alkemade, Appl. Catal. A: General 115 (1994) 103–120.
[17] L. Kubelková, V. Seidl, G. Borbély, H.K. Beyer, J. Chem. Soc., Faraday Trans. 1 84(5) (1988) 1447–1454.
[18] J.P. Gilson, G.C. Edwards, A.W. Peters, K. Rajagopalan, R.F. Wormsbecher, T.G. Roberie, M.P. Shatlock, J. Chem. Soc., Chem. Commun. (1987) 91–92.
[19] L. Kellberg, M. Linsten, H.J. Jakobsen, Chem. Phys. Lett. 182 (1991) 120–126.
[20] H.G. Karge, V. Dondur, J. Weitkamp, J. Phys. Chem. 95 (1991) 283–288.
[21] W.O. Haag, R.M. Dessau, Proc. 8th. Int. Congr. Catal., vol. II (1984) 305–316.
[22] A. Corma, J. Planelles, J. Sanchez-Marin, F. Tomas, J. Catal. 93 (1985) 30–37.
[23] P.O. Fritz, J.H. Lunsford, J. Catal. 118 (1989) 85–98.
[24] R. Carvajal, P.J. Chu, J.H. Lunsford, J. Catal. 125 (1990) 123–131.